

# Geophysical Research Letters

## RESEARCH LETTER

10.1029/2020GL092305

### Key Points:

- Particle-in-cell (PIC) simulations demonstrate whistler-mode waves can be trapped inside the enhanced density ducts which can interpret satellite observations
- These trapped waves remain quasi-parallel and get much larger amplitudes during propagation toward high latitudes
- These trapped waves focus at a spatially narrow channel inside the enhanced density ducts

### Supporting Information:

- Supporting Information S1

### Correspondence to:

X. Gao and L. Chen,  
[gaoxl@mail.ustc.edu.cn](mailto:gaoxl@mail.ustc.edu.cn);  
[lunjin.chen@gmail.com](mailto:lunjin.chen@gmail.com)

### Citation:

Ke, Y., Chen, L., Gao, X., Lu, Q., Wang, X., Chen, R., et al. (2021). Whistler-mode waves trapped by density irregularities in the Earth's magnetosphere. *Geophysical Research Letters*, 48, e2020GL092305. <https://doi.org/10.1029/2020GL092305>

Received 26 DEC 2020

Accepted 26 FEB 2021

© 2021. American Geophysical Union.  
 All Rights Reserved.

## Whistler-Mode Waves Trapped by Density Irregularities in the Earth's Magnetosphere

Yangguang Ke<sup>1,2</sup> , Lunjin Chen<sup>3</sup> , Xinliang Gao<sup>1,2</sup> , Quanming Lu<sup>1,2</sup> , Xueyi Wang<sup>4</sup> , Rui Chen<sup>1,2</sup> , Huayue Chen<sup>1,2</sup> , and Shui Wang<sup>1,2</sup>

<sup>1</sup>CAS Key Laboratory of Geospace Environment, Department of Geophysics and Planetary Science, University of Science and Technology of China, Hefei, China, <sup>2</sup>CAS Center for Excellence in Comparative Planetology, Hefei, China, <sup>3</sup>Department of Physics, University of Texas at Dallas, Richardson, TX, USA, <sup>4</sup>Department of Physics, Auburn University, Auburn, AL, USA

**Abstract** Whistler-mode waves are electromagnetic waves pervasively observed in the Earth's and other planetary magnetospheres. They are considered to be mainly responsible for producing the hazardous radiation and diffuse aurora, which heavily relies on their properties. Density irregularities, frequently observed in the Earth's magnetospheres, are found to change largely the properties of whistler-mode waves. Here we report, using Van Allen Probes measurements, whistler-mode waves strongly modulated by two different density enhancements. With particle-in-cell simulations, we propose wave trapping caused by field-aligned density irregularities (ducts) may account for this phenomenon. Simulation results show that whistler-mode waves can be trapped inside the enhanced density ducts. These trapped waves remain quasi-parallel and usually get much larger amplitudes than those unducted whistler waves during propagation away from the magnetic equator, and tend to focus at a spatially narrow channel, consistent with observations. Our results imply density irregularities may be significant to modulate radiation-belt electrons.

### 1. Introduction

Whistler-mode waves are commonly observed in space plasma environments and laboratory plasma experiments (Van Compernelle et al., 2015), which occur naturally in the Earth's magnetosphere (Burtis & Helliswell, 1969; Gao et al., 2014; Horne, 2005; Meredith et al., 2001; Tsurutani & Smith, 1974, 1977) and other magnetized planets (Harada et al., 2016; Horne et al., 2008; Hospodarsky et al., 2008). They are primarily responsible for producing the planetary radiation belts (Horne et al., 2005, 2008; Thorne et al., 2013) and auroral precipitation (Kasahara et al., 2018; Ni et al., 2008; Nishimura et al., 2010; Thorne et al., 2010) via accelerating and scattering electrons. Whistler-mode waves were first discovered on the ground over a century ago (Preece, 1894), and were since frequently observed by ground-based detections (Stenzel, 1999). The existence of Earth-magnetosphere/ionosphere waveguide is widely accepted, which guides whistler-mode waves to reach the ground (Ohta et al., 1996; Stenzel, 1999). The most common waveguides are field-aligned density irregularities (also called density ducts) supported by theoretical and numerical works (Hanzelka & Santolík, 2019; Smith et al., 1960; Streltsov et al., 2006), which have been frequently detected by satellite-based measurements (Carpenter et al., 2002; Darrouzet et al., 2009) and ground-based imaging telescope (Loi et al., 2015). Density ducts can guide whistler-mode waves, which naturally lead to modulations of whistler-mode wave properties.

The properties of whistler-mode waves are essential to mediate energetic electron fluxes in the radiation belt (Artemyev et al., 2015; Mourenas et al., 2012), which have been thoroughly studied by satellite observations (Agapitov et al., 2013; Li et al., 2013; Santolík et al., 2014; Shue et al., 2019) and kinetic simulation in a dipole magnetic field (Lu et al., 2019). The whistler-mode waves are primarily emitted at the equatorial region (Lauben et al., 2002; LeDocq et al., 1998; Li et al., 2013; Santolík et al., 2005), and their wave normal angles become larger when propagating toward the higher latitude (Breuillard et al., 2012; Hanzelka & Santolík, 2019; Lu et al., 2019). However, how whistler-mode waves emit and propagate self-consistently in density ducts is still unknown. Here we present whistler-mode waves strongly modulated by two different density enhancements observed by Van Allen Probe measurements. With two-dimensional kinetic

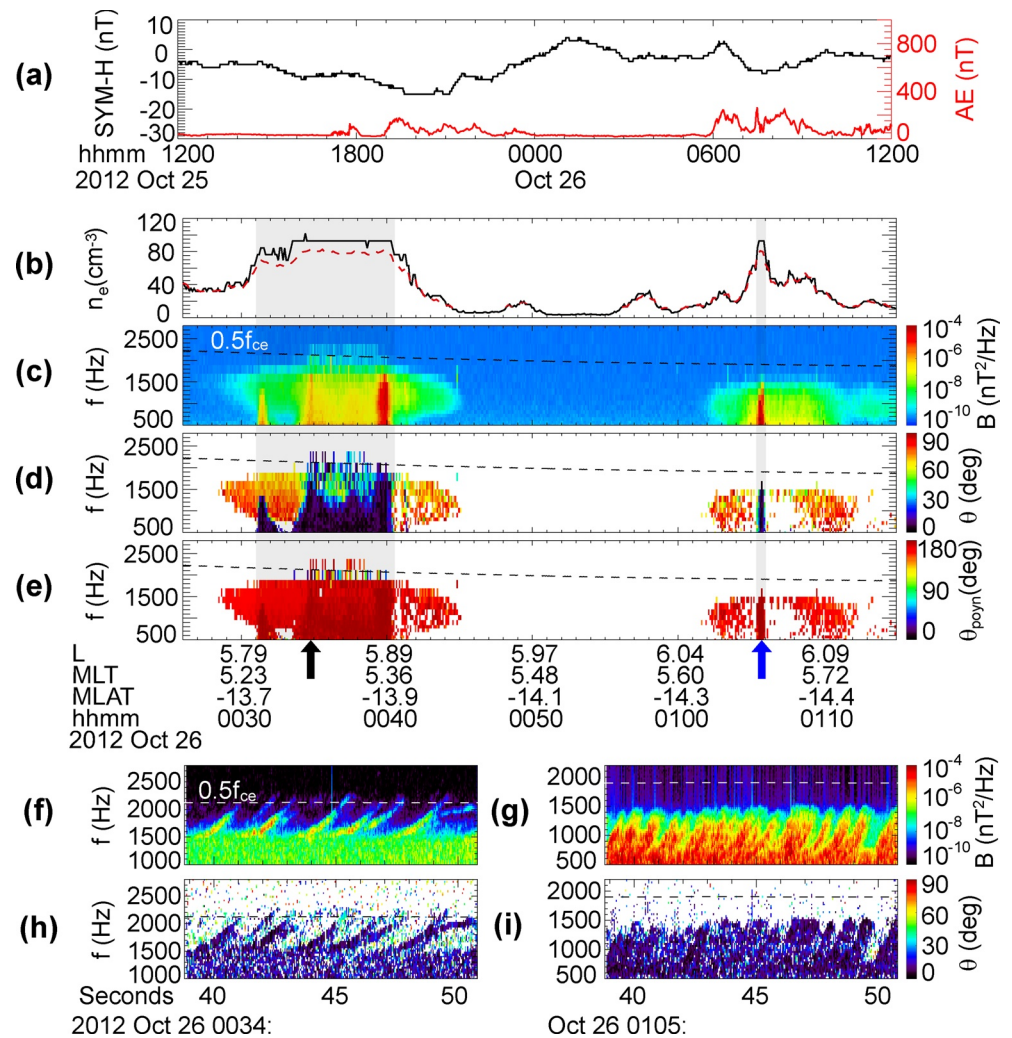


**Figure 1.** (a) The SYM-H index and AE index. (b) The electron number density inferred from the spacecraft potential (dashed line) and the upper hybrid frequency (solid line) detected by RBSP-A. (c) Magnetic spectral intensity of chorus waves from the EMFISIS instrument. (d) The wave normal angles calculated from the waveform data. (e) The angles between the background magnetic field and the Poynting vectors. (f) and (g) The high-cadence wave dynamic spectra in the time durations marked by the black and blue arrows. (h) and (i) The corresponding wave normal angles. Only the angles corresponding to the polarization ratio > 0.6 and the ellipticity > 0.7 are displayed.

simulations in a dipole magnetic field, we present the properties of whistler-mode waves trapped by enhanced density ducts, which are similar to above observations.

## 2. Observation and Data Analysis

During a quiet period of geomagnetic activity indicated by SYM-H and AE index (Figure 1a), Van Allen Probe-A (Mauk et al., 2013) detects whistler-mode waves in two density enhancements at  $L \sim 6$  and magnetic latitude (LAT)  $\sim -14^\circ$  in the dawnside on October 26, 2012 (Figures 1b and 1c), where  $L$  is the equatorial radial distance of the geomagnetic field in units of Earth Radius  $R_E$ . The electron number density  $n_e$ , inferred from the spacecraft potential (Wygant et al., 2013) (dashed line) and the upper hybrid frequency (Kurth et al., 2015) (solid line), shows two density enhancements with different shapes and sizes (Figure 1b). We call them as flat-topped and bell-shaped density enhancements, respectively. Whistler-mode waves are detected by the waveform receiver instrument (Kletzing et al., 2013) over a frequency range below  $0.5f_{ce}$ , where  $f_{ce}$  is the equatorial electron gyrofrequency. These whistler waves inside the density

enhancements are mostly intense and quasi-parallel with wave normal angles  $\theta < 30^\circ$ , while these waves outside the density enhancements are weak and very oblique (Figures 1c and 1d), where  $\theta$  is calculated by the singular value decomposition (SVD) method (Santolík et al., 2003). There are also some highly oblique whistler mode waves observed inside the density enhancement, which may be from outside since they can freely penetrate into the density enhancement (Streltsov et al., 2006) or locally excited (Li et al., 2016). Most interestingly, these quasi-parallel whistler waves have much larger amplitudes in the narrow regions inside both density enhancements: the region near the outer boundary inside the flat-topped density enhancement and the region in the center of the bell-shaped density enhancement (Figure 1c). The angles  $\theta_{\text{poynt}}$  between the Poynting vectors and the background magnetic field reveal that these waves propagate southward away from the equatorial region (Figure 1e). The high-cadence wave dynamic spectra (Figures 1f and 1g) corresponding to the durations marked by the black and blue arrows, present that rising-tone chorus waves with small wave normal angles appear in both density enhancements (Figures 1h and 1i). Some information of the observed hot electrons during this event are presented in Figure S1 in the supporting information.

The two density enhancements may be field-aligned density structures (ducts) due to diffusive equilibrium (Bortnik et al., 2011). Their peak number densities are about  $90 \text{ cm}^{-3}$  and the surrounding number densities are about  $40 \text{ cm}^{-3}$ . The equatorial radial widths of the regions where these quasi-parallel whistler waves appear (marked by shadows) are  $\sim 580 \text{ km}$  (equal to tens of wavelengths  $\lambda_w$  of a quasi-parallel whistler wave at  $0.2f_{ce}$ ) inside the flat-topped density enhancement and  $\sim 25 \text{ km}$  (several wavelengths  $\lambda_w$ ) inside the bell-shaped density enhancement.

### 3. Simulations of Whistler-Mode Waves in Density Ducts

#### 3.1. Simulation Setup

We carry out two self-consistent particle-in-cell simulations to study the dynamics of whistler waves in the flat-topped and bell-shaped density ducts. The two-dimensional (2-D) general curvilinear particle-in-cell (gcPIC) code is used in this paper, which had been successful in studying excitation and propagation of whistler-mode chorus waves in the Earth's space plasma environments (Ke et al., 2017; Lu et al., 2019). The 2-D gcPIC model allows three-dimensional electromagnetic fields and velocities but only 2-D spatial variations on the magnetic meridian plane. A dipole field is used as the background magnetic field and the field line can be expressed as  $p=r/\cos^2\lambda$ , where  $p$  is the distance from the magnetic equator to the Earth's center,  $r$  is the distance of the point to the Earth's center and  $\lambda$  is the magnetic latitude. The regions at  $L \sim 6$  with ambient densities  $n_0 \approx 40 \text{ cm}^{-3}$  are corresponding to  $p \approx 45,500d_{e0}$  ( $d_{e0} = c / \omega_{pe}$  is electron inertial length and  $\omega_{pe} = \sqrt{n_0 e^2 / m_e \epsilon_0}$  is electron plasma frequency, where  $c$  is the speed of light,  $e$  represents the elementary charge,  $m_e$  is the mass of the electron and  $\epsilon_0$  is the permittivity vacuum), which is too large and thus requires too expensive computation resources. Hence we use a scaling simulation domain of  $p = 2,500d_{e0} - 2,800d_{e0}$  and  $\lambda \approx -30^\circ - 30^\circ$ . The value of  $\omega_{pe} / \Omega_{e0} = 14$  consistent with the observations is applied, where electron gyrofrequency  $\Omega_{e0} = eB_{0eq,m} / m_e$  and  $B_{0eq,m}$  is the magnetic field on the location ( $p = 2,650d_{e0}$ ,  $\lambda = 0^\circ$ ). There are two electron components: cold background electrons and anisotropic hot electrons for exciting whistler waves (Kennel & Petschek, 1966; Li et al., 2010; Tsurutani & Smith, 1974). A fixed ion background is setup to ensure plasma charge neutrality. The cold electrons are treated as a fluid with number density  $n_e$  which is set equal along the same field line. We set up the density ducts by changing  $n_e$  in the direction perpendicular to the magnetic field. For the flat-topped density duct in simulation case 1, its flat-topped part has  $n_e = n_I$  and the equatorial radial width  $D = 80d_{e0}$ . Its inner and outer boundaries are set by the modified Gaussian function

$$n_e = n_0 + (n_I - n_0) \exp\left[-\frac{p'^2}{2\rho^2}\right], \quad (1)$$

where  $n_0$  represents the background density outside the duct,  $\rho = 10d_{e0}$  is the characteristic scale, and  $p'$  indicates  $p - p_1$  ( $p_1 = 2610d_{e0}$ ) for the inner boundary and  $p - p_2$  ( $p_2 = 2,690d_{e0}$ ) for the outer boundary respectively. The bell-shaped density duct in simulation case 2 is also set by Equation 1 with  $p' = p - p_3$

( $p_3 = 2,650d_{e0}$ ). We set  $n_I = 2n_0$ , since the peak number densities  $\sim 90 \text{ cm}^{-3}$  in both observed density enhancements are approximately twice the outside densities  $\sim 40 \text{ cm}^{-3}$ .

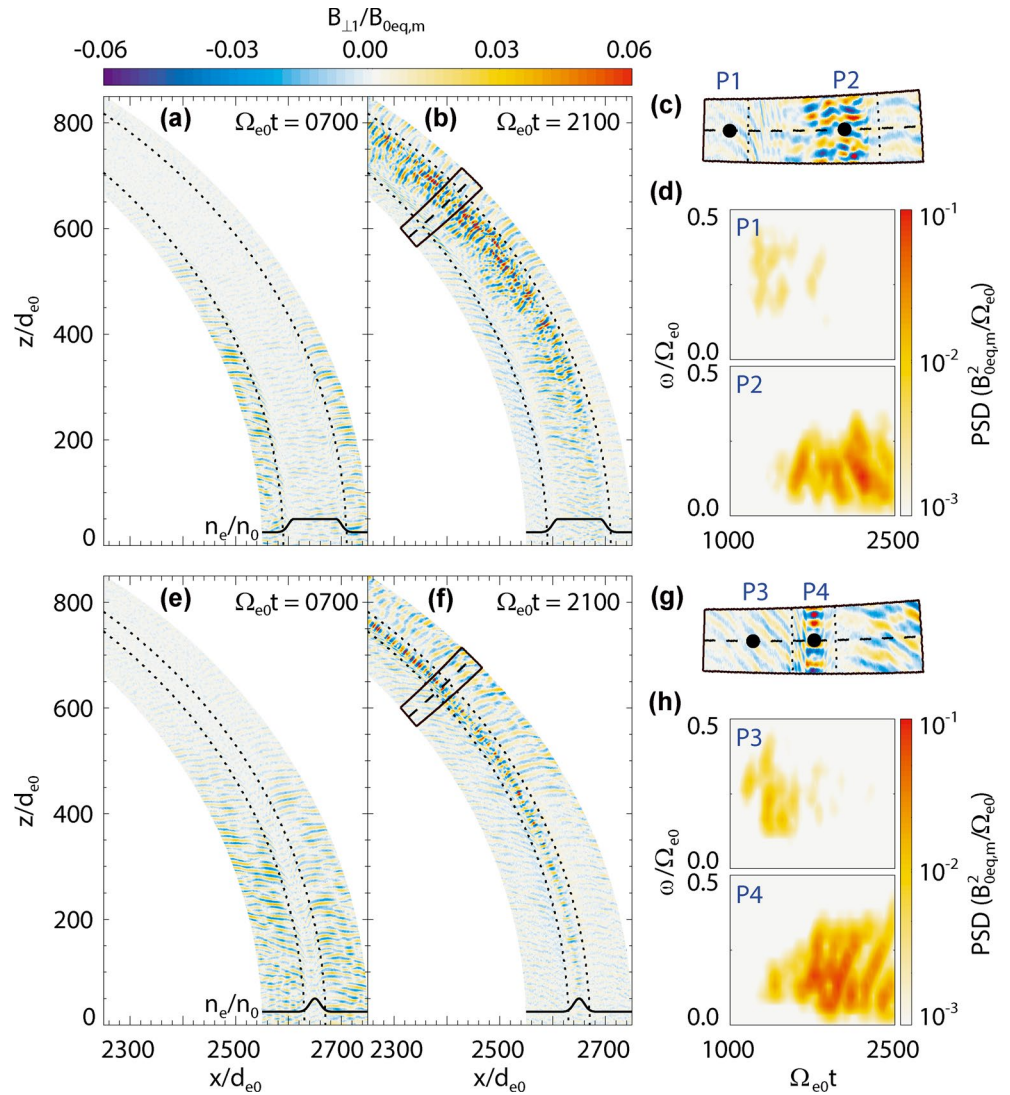
For simplicity, the hot electrons adopt a bi-Maxwellian distribution with temperature anisotropy  $T_{h\perp} / T_{h\parallel} = 4$ , number density  $n_h / n_0 = 0.01$ , and parallel thermal velocity  $v_{th\parallel} = 0.09c$  at the magnetic equator. The parallel thermal velocity is corresponding to  $\sim 2 \text{ keV}$  close to the observed values (Figure S1). The temperature anisotropy is larger than observed values to easily generate waves in the simulations. Off the magnetic equator, hot electron distribution can be derived from Liouville's theorem (Summers et al., 2012). The simulation grid numbers are  $N_{\parallel} = 4,000$  along the field lines and  $N_{\perp} = 300$  along the curves orthogonal to the field lines. The time step is  $\Omega_{e0}\Delta t = 0.04$ . A total of about 1.2 billion superparticles are used for hot electrons. The boundary conditions are absorbing boundary conditions for waves and reflecting boundary conditions for particles (Lu et al., 2019).

### 3.2. Simulation Results

The overview of simulation results displaying spatial-temporal evolution of excited whistler waves is shown in Figure 2. The spatial profiles of perpendicular (to the simulation plane) magnetic fluctuations  $B_{\perp 1} / B_{0eq,m}$  in the Cartesian coordinates ( $x, z$ ) at  $\Omega_{e0}t = 700$  and 2,100 are presented for simulation case 1 (Figures 2a and 2b) and case 2 (Figures 2e and 2f). The black solid line indicates the distribution of cold electron density on  $x$  at  $z = 0$ , and the dotted lines mark the edges of the density duct. The equatorial radial widths are defined as  $D + 4\rho = 120d_{e0}$  for the flat-topped duct and  $4\rho = 40d_{e0}$  for the bell-shaped duct, equal to  $\sim 10 \lambda_w$  and several  $\lambda_w$  respectively. The dashed line with central point near  $\lambda = 15^\circ$  is orthogonal to the field lines. The whistler waves are initially excited near the magnetic equator, and these waves inside the duct are weaker than that outside the duct (Figures 2a and 2e), which can be explained by the linear growth rates. During off-equatorial propagation, these whistler waves outside the ducts attenuate significantly at high latitudes, while these waves inside the ducts are trapped by the duct boundaries and become much more intense even at  $\lambda > 15^\circ$  (Figures 2b and 2f). Besides, these trapped waves gather near the outer boundary of the broad flat-topped duct and in the center of the narrow bell-shaped duct. The regions bounded by the approximate rectangles (Figures 2b and 2f) are zoomed in (Figures 2c and 2g), which show quasi-parallel wave packets inside the ducts and oblique wave packets outside the ducts. Figure 2d (2h) displays wave dynamic spectra at the locations P1 and P2 (P3 and P4) marked by two black dots in Figure 2c (2g), showing that the whistler waves trapped inside the ducts are much stronger than outside waves at high latitudes due to the less Landau damping and more nonlinear growth.

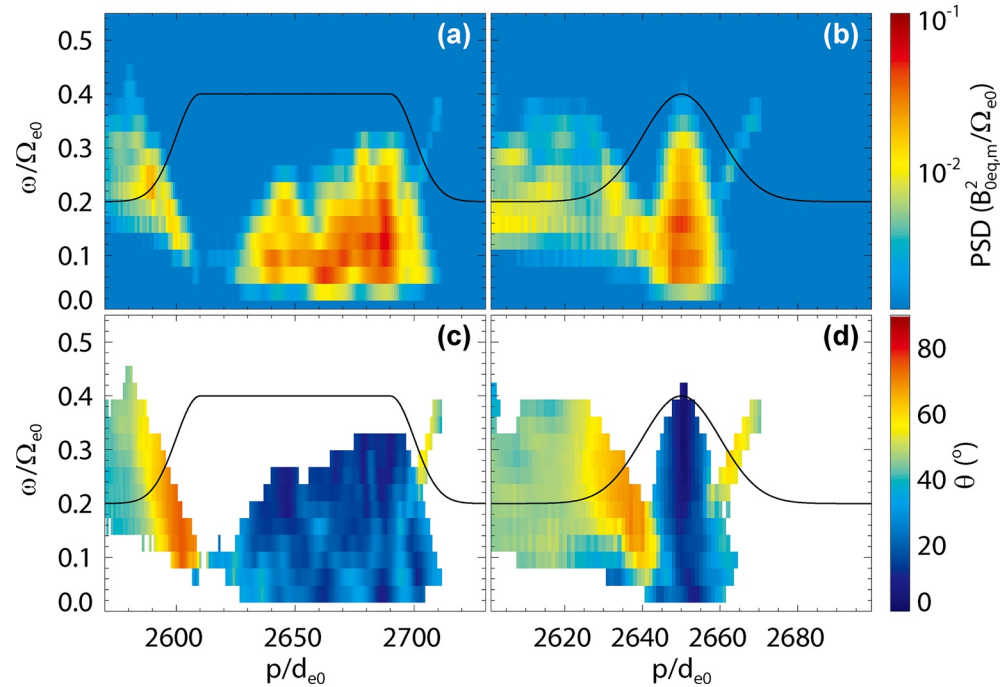
Figure 3 exhibits the wave power spectral density (PSD) of magnetic field fluctuations along the paths indicated by the dashed lines in Figures 2c and 2g. The wave power spectral densities are integrated over the full simulation duration ( $\Omega_{e0}t = 0-2,500$ ). The wave normal angles  $\theta$  are obtained by SVD method (Santolík et al., 2003) and weighted by the PSD. Figures 3a and 3b show that PSD of whistler waves inside the ducts are much higher than that outside the ducts. These waves inside the ducts are mostly quasi-parallel with small  $\theta$  while these waves outside are oblique with large  $\theta$  up to  $\sim 75^\circ$  (Figures 3c and 3d). However, a small portion of highly oblique waves appear inside the density ducts near the boundaries, consistent with the observations. These very oblique waves are from the outside, which can penetrate into the enhanced density duct also predicted by the ducting theory (Streltsov et al., 2006). In addition, the more intense whistler waves appear around the outer boundary of the flat-topped duct but in the center of the bell-shaped duct. These results are well consistent with the observations.

Figure 4 presents the spatial profiles of the absolute values of  $B_{\perp 1} / B_{0eq,m}$  at  $\Omega_{e0}t = 1,800, 1,900$ , and 2,000 for simulation case 1. Inside the density duct, a wave packet at different times is circled by blue ellipses (Figures 4a-4c). This wave packet is initially on the field line L1 at  $\Omega_{e0}t = 1,800$ , and then propagate toward high latitude and refract outward. It reaches the region outside the field line L1 at  $\Omega_{e0}t = 2,000$ . The outward propagation of these waves are mainly due to the magnetic field curvature, consistent with ray tracing simulations (Breuillard et al., 2012; Chen et al., 2013) and observation statistics (Santolík et al., 2010; Taubenschuss et al., 2016). This can explain why waves gather near the outer boundary inside the flat-topped density duct.



**Figure 2.** The spatial profiles of perpendicular magnetic field fluctuations  $B_{\perp 1} / B_{0eq,m}$  (perpendicular to the simulation plane) in the Cartesian coordinates  $(x, z)$  at  $\Omega_{e0}t = 700$  and  $2,100$  for (a) and (b) simulation case 1, and (e) and (f) simulation case 2. The black solid lines indicate the radial profiles of cold electron density along  $x$  at  $z = 0$ , and two dotted lines mark the edges of the density duct. (c) and (g) The enlarged view of the regions bounded by the approximate rectangles in Figures 2b and 2f. (d) and (h) Wave dynamic spectra at the locations P1, P2, P3, and P4 marked by black dots in Figures 2c and 2g.

To better understand the effects of the enhanced density duct on waves, we performed one additional simulation (case 3) with cold electron density  $n_e = 2n_0$ . The other simulation parameters are same as that in simulation case 1. The spatial profiles of  $B_{\perp 1} / B_{0eq,m}$  in simulation case 1 and case 3 at  $\Omega_{e0}t = 2,000$  are presented in Figures 5a and 5b, respectively. The same field line  $p = 2,680d_{e0}$  is marked by black line in Figure 5a and blue line in Figure 5b. The PSD on each point along this field line integrated over  $\Omega_{e0}t = 0-2,500$  and  $\omega / \Omega_{e0} = 0.1-0.3$  in case 1 (black line) and case 3 (blue line) are displayed in Figure 5c. The corresponding wave normal angles (weighted by PSD) are presented in Figure 5d. Just as expected, under the same initial conditions, the whistler mode waves trapped inside the enhanced density duct remain quasi-parallel and more intense than those unducted waves off the equator (Figures 5c and 5d).



**Figure 3.** (a) and (b) The wave power spectral density (PSD) of magnetic field fluctuations along the paths indicated by the dashed lines in Figures 2c and 2g. (c) and (d) The corresponding wave normal angles  $\theta$  weighted by the PSD. The PSD and  $\theta$  are integrated over the full simulation duration ( $\Omega_{e0}t = 0-2,500$ ).

#### 4. Discussion and Conclusions

Through Van Allen Probe data, we report one event that whistler-mode waves have markedly different properties between inside and outside the density enhancements. Whistler-mode waves inside the density enhancements are mainly quasi-parallel and much stronger than those outside waves that are very oblique. The density enhancements up to  $90 \text{ cm}^{-3}$  at  $L \sim 6$  are likely to be parts of a plume (Shi et al., 2019; Su et al., 2018), which can be narrow on the dawnside (Zhang et al., 2019). Actually, we have found a

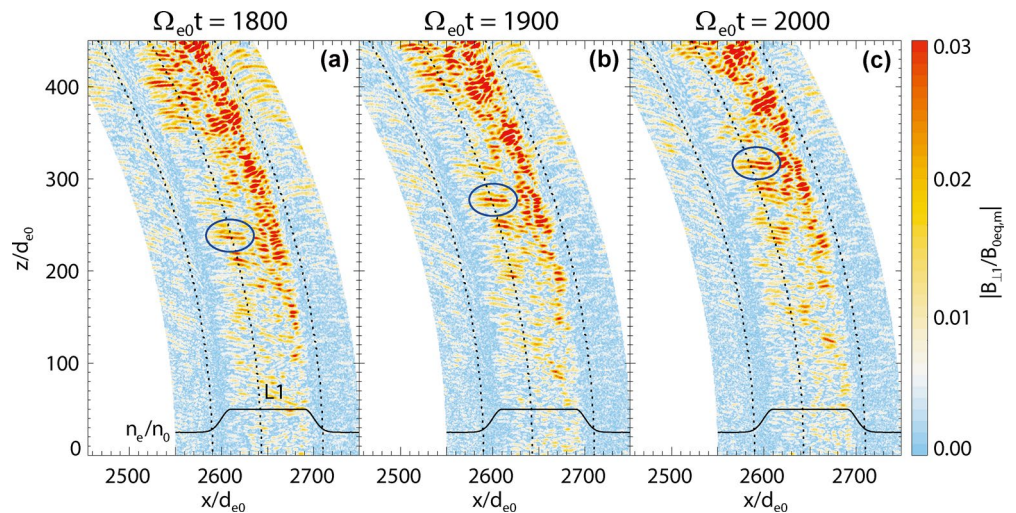


**Figure 4.** The spatial profiles of the absolute values of  $B_{\perp 1} / B_{0eq,m}$  at (a-c)  $\Omega_{e0}t = 1,800, 1,900$ , and  $2,000$  for simulation case 1. The dotted line L1 represents a reference magnetic field line. The same wave packets at different times are marked by the blue ellipses.

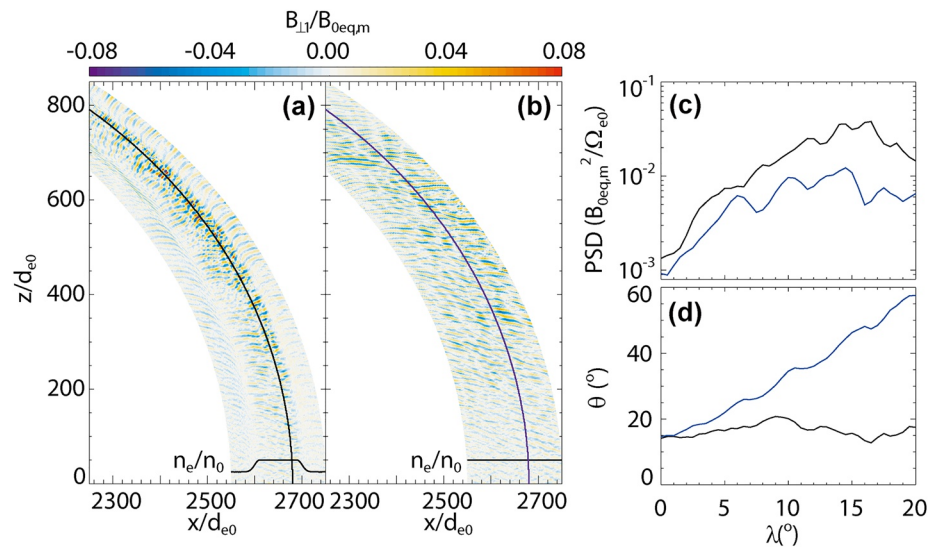


**Figure 5.** The spatial profiles of  $B_{\perp 1} / B_{0eq,m}$  in simulation case 1 (a) and case 3 (b) at  $\Omega_{e0}t = 2,000$ . The black line and blue line mark the same field line  $p = 2,680d_{e0}$ . (c) The power spectral density (PSD) on each point along this field line integrated over  $\Omega_{e0}t = 0-2,500$  and  $\omega / \Omega_{e0} = 0.1-0.3$  in case 1 (black line) and case 3 (blue line). (d) The corresponding wave normal angles (weighted by PSD) in case1 (black line) and case 3 (blue line).

number of similar events detected by Van Allen Probes near dawn, and also shown another one in the supporting information (Figure S2). The large-amplitude whistler waves in the plumes are thought to be qualitatively explained by the linear theory through assuming whistler waves are parallel-propagating (Su et al., 2018). The larger linear growth rates is considered to be a probable cause of intensification of whistler-mode waves in density enhancements (Li et al., 2011). However, in this event, the whistler waves inside the density enhancements remain quasi-parallel at higher latitudes, which is not expected in a dipole magnetic field without the ducting effect. In our simulations, these waves outside the density ducts will become more oblique and experience strong Landau damping, while those inside ducted waves can remain quasi-parallel and gain more nonlinear growth. The simulations coincide with the observations very well.

Whistler-mode waves trapped (guided) by density ducts have been studied by ray-tracing simulations (Hanzelka & Santolík, 2019; Smith et al., 1960) and electron magnetohydrodynamics simulations (Streltsov et al., 2006, 2007). However, both methods are unable to reproduce wave excitation and nonlinear interactions with particles, which play a key role in wave evolution and the radiation belt dynamics. Therefore, we carried out 2-D kinetic simulations in a dipole magnetic field to study how whistler waves generate and evolve in the density ducts. Our simulation results show that whistler waves usually propagate toward high latitudes and refract outward in a dipole magnetic field due to the magnetic field curvature (Figure 4). Thus, these whistler waves inside the broad flat-topped density duct tend to move toward the outer boundary and will experience inward refraction when reaching the outer boundary because of high density gradient, resulting in wave congregating and propagating nearly along the field-aligned outer boundary. These whistler waves inside the narrow bell-shaped density duct are refracted by inner and outer boundaries (Smith et al., 1960), leading to wave concentrating and propagating in the central region of the duct. We also call that these whistler waves are trapped (guided) by the enhanced density ducts. These trapped waves are much intense than those unducted waves. First, these waves from different places are trapped in a spatially narrow channel, leading to concentration of wave energy. Second, these trapped waves remain quasi-parallel, thus undergo less Landau damping. Third, these trapped waves may get much more nonlinear growth due to the larger amplitude (Omura et al., 2009). Our simulation results show that these properties of the whistler waves trapped by the enhanced density ducts are well consistent with that in the observed density enhancements. Our main conclusions are as follows:

1. Whistler-mode waves can be trapped inside the enhanced density ducts and remain quasi-parallel propagating supported by satellite observations and PIC simulations.
2. These trapped whistler-mode waves usually get much larger amplitudes than those waves outside the enhanced density ducts during propagation toward high latitudes due to less Landau damping, focusing effect, and more nonlinear growth.
3. These trapped whistler-mode waves generally focus at a spatially narrow channel inside the enhanced density ducts due to the effects of magnetic field curvature and density gradient.

Whistler-mode waves, ubiquitous in planetary plasma space, play a key role in controlling energetic electron fluxes in the planetary radiation belt, which are highly regulated by the properties of whistler waves. The density irregularities, observed frequently in the radiation belt, are found to change largely the properties of whistler waves in present study, which may play an important role in modulating energetic electron fluxes in the radiation belt. Studying the effects of the trapped whistler waves on energetic electrons will be left for a future work.

### Data Availability Statement

The Van Allen Probe data are publicly available from the website <https://spdf.gsfc.nasa.gov/pub/data/rbsp/>. The SYM-H and AE index data are publicly available from the OMNI website (<https://omniweb.gsfc.nasa.gov>). Simulation datasets for this research are available at the following link <http://doi.org/10.5281/zenodo.3859476>.

### Acknowledgments

This work is supported by the B-type Strategic Priority Program of the Chinese Academy of Sciences (XDB41000000), Key Research Program of Frontier Sciences, CAS(QYZDJ-SSW-DQC010), the National Science Foundation of China (NSFC) grants (41774169), and the Fundamental Research Funds for the Central Universities. The authors acknowledge the entire Van Allen Probes instrument group. In particular, the authors would like to thank Craig A. Kletzing for providing the data of EMFISIS and J. R. Wygant for providing the data of EFW. The PIC simulations were carried out at National Supercomputer Center in Tianjin, and the calculations were performed on TianHe-1 (A).

### References

- Agapitov, O., Artemyev, A., Krasnoselskikh, V., Khotyaintsev, Y. V., Mourenas, D., Breuillard, H., et al. (2013). Statistics of whistler mode waves in the outer radiation belt: Cluster STAFF-SA measurements. *Journal of Geophysical Research Space Physics*, *118*(6), 3407–3420. <https://doi.org/10.1002/jgra.50312>
- Artemyev, A. V., Agapitov, O. V., Mourenas, D., Krasnoselskikh, V. V., & Mozer, F. S. (2015). Wave energy budget analysis in the Earth's radiation belts uncovers a missing energy. *Nature Communications*, *6*, 8143. <https://doi.org/10.1038/ncomms8143>
- Bortnik, J., Chen, L., Li, W., Thorne, R. M., & Horne, R. B. (2011). Modeling the evolution of chorus waves into plasmaspheric hiss. *Journal of Geophysical Research*, *116*, A08221. <https://doi.org/10.1029/2011ja016499>
- Breuillard, H., Zaliznyak, Y., Krasnoselskikh, V., Agapitov, O., Artemyev, A., & Rolland, G. (2012). Chorus wave-normal statistics in the Earth's radiation belts from ray tracing technique. *Annales Geophysicae*, *30*(8), 1223–1233. <https://doi.org/10.5194/angeo-30-1223-2012>
- Burtis, W. J., & Helliwell, R. A. (1969). Banded chorus-A new type of VLF radiation observed in the magnetosphere by OGO 1 and OGO 3. *Journal of Geophysical Research*, *74*(11), 3002–3010. <https://doi.org/10.1029/ja074i011p03002>
- Carpenter, D. L., Spasojevic, M. A., Bell, T. F., Inan, U. S., Reinisch, B. W., Galkin, I. A., et al. (2002). Small-scale field-aligned plasmaspheric density structures inferred from the Radio Plasma Imager on IMAGE. *Journal of Geophysical Research*, *107*(A9). <https://doi.org/10.1029/2001ja009199>
- Chen, L., Thorne, R. M., Li, W., & Bortnik, J. (2013). Modeling the wave normal distribution of chorus waves. *Journal of Geophysical Research Space Physics*, *118*(3), 1074–1088. <https://doi.org/10.1029/2012ja018343>
- Darrouzet, F., Gallagher, D. L., André, N., Carpenter, D. L., Dandouras, I., Décréau, P. M., et al. (2009). Plasmaspheric density structures and dynamics: Properties observed by the cluster and image missions. In F. Darrouzet, J. De Keyser, & V. Pierrard (Eds.), *The Earth's plasmasphere: A cluster and image perspective* (pp. 55–106). New York, NY: Springer New York.
- Gao, X., Li, W., Thorne, R. M., Bortnik, J., Angelopoulos, V., Lu, Q., et al. (2014). New evidence for generation mechanisms of discrete and hiss-like whistler mode waves. *Geophysical Research Letters*, *41*(14), 4805–4811. <https://doi.org/10.1002/2014gl060707>
- Hanzelka, M., & Santolik, O. (2019). Effects of ducting on whistler mode chorus or exohiss in the outer radiation belt. *Geophysical Research Letters*, *46*(11), 5735–5745. <https://doi.org/10.1029/2019gl083115>
- Harada, Y., Andersson, L., Fowler, C. M., Mitchell, D. L., Halekas, J. S., Mazelle, C., et al. (2016). MAVEN observations of electron-induced whistler mode waves in the Martian magnetosphere. *Journal of Geophysical Research: Space Physics*, *121*(10), 9717–9731. <https://doi.org/10.1002/2016ja023194>
- Horne, R. B. (2005). Timescale for radiation belt electron acceleration by whistler mode chorus waves. *Journal of Geophysical Research*, *110*(A3), A03225. <https://doi.org/10.1029/2004ja010811>
- Horne, R. B., Thorne, R. M., Glauert, S. A., Douglas Menietti, J., Shprits, Y. Y., & Gurnett, D. A. (2008). Gyro-resonant electron acceleration at Jupiter. *Nature Physics*, *4*(4), 301–304. <https://doi.org/10.1038/nphys897>
- Horne, R. B., Thorne, R. M., Shprits, Y. Y., Meredith, N. P., Glauert, S. A., Smith, A. J., et al. (2005). Wave acceleration of electrons in the Van Allen radiation belts. *Nature*, *437*(7056), 227–230. <https://doi.org/10.1038/nature03939>
- Hospodarsky, G. B., Averkamp, T. F., Kurth, W. S., Gurnett, D. A., Menietti, J. D., Santolik, O., & Dougherty, M. K. (2008). Observations of chorus at Saturn using the Cassini Radio and Plasma Wave Science instrument. *Journal of Geophysical Research*, *113*(A12), A12206. <https://doi.org/10.1029/2008ja013237>
- Kasahara, S., Miyoshi, Y., Yokota, S., Mitani, T., Kasahara, Y., Matsuda, S., et al. (2018). Pulsating aurora from electron scattering by chorus waves. *Nature*, *554*(7692), 337–340. <https://doi.org/10.1038/nature25505>
- Kennel, C. F., & Petschek, H. E. (1966). Limit on stably trapped particle fluxes. *Journal of Geophysical Research*, *71*(1), 1–28. <https://doi.org/10.1029/jz071i001p00001>
- Ke, Y., Gao, X., Lu, Q., Wang, X., & Wang, S. (2017). Generation of rising-tone chorus in a two-dimensional mirror field by using the general curvilinear PIC code. *Journal of Geophysical Research: Space Physics*, *122*(8), 8154–8165. <https://doi.org/10.1002/2017ja024178>

- Kletzing, C. A., Kurth, W. S., Acuna, M., MacDowall, R. J., Torbert, R. B., Averkamp, T., et al. (2013). The Electric and Magnetic Field Instrument Suite and Integrated Science (EMFISIS) on RBSP. *Space Science Reviews*, 179(1–4), 127–181. <https://doi.org/10.1007/s11214-013-9993-6>
- Kurth, W. S., De Pascuale, S., Faden, J. B., Kletzing, C. A., Hospodarsky, G. B., Thaller, S., & Wygant, J. R. (2015). Electron densities inferred from plasma wave spectra obtained by the Waves instrument on Van Allen Probes. *Journal of Geophysical Research: Space Physics*, 120(2), 904–914. <https://doi.org/10.1002/2014ja020857>
- Lauben, D. S., Inan, U. S., Bell, T. F., & Gurnett, D. A. (2002). Source characteristics of ELF/VLF chorus. *Journal of Geophysical Research: Space Physics*, 107(A12), 1429. SMP 10-11-SMP 10-17. <https://doi.org/10.1029/2000ja003019>
- LeDocq, M. J., Gurnett, D. A., & Hospodarsky, G. B. (1998). Chorus source locations from VLF Poynting flux measurements with the Polar spacecraft. *Geophysical Research Letters*, 25(21), 4063–4066. <https://doi.org/10.1029/1998gl900071>
- Li, W., Bortnik, J., Thorne, R. M., Cully, C. M., Chen, L., Angelopoulos, V., et al. (2013). Characteristics of the Poynting flux and wave normal vectors of whistler-mode waves observed on THEMIS. *Journal of Geophysical Research: Space Physics*, 118(4), 1461–1471. <https://doi.org/10.1002/jgra.50176>
- Li, W., Bortnik, J., Thorne, R. M., Nishimura, Y., Angelopoulos, V., & Chen, L. (2011). Modulation of whistler mode chorus waves: 2. Role of density variations. *Journal of Geophysical Research*, 116(A6), A06206. <https://doi.org/10.1029/2010ja016313>
- Li, W., Mourenas, D., Artemyev, A. V., Bortnik, J., Thorne, R. M., Kletzing, C. A., et al. (2016). Unraveling the excitation mechanisms of highly oblique lower band chorus waves. *Geophysical Research Letters*, 43(17), 8867–8875. <https://doi.org/10.1002/2016gl070386>
- Li, W., Thorne, R. M., Nishimura, Y., Bortnik, J., Angelopoulos, V., McFadden, J. P., et al. (2010). THEMIS analysis of observed equatorial electron distributions responsible for the chorus excitation. *Journal of Geophysical Research*, 115(A6), A00F11. <https://doi.org/10.1029/2009ja014845>
- Loi, S. T., Murphy, T., Cairns, I. H., Menk, F. W., Waters, C. L., Erickson, P. J., et al. (2015). Real-time imaging of density ducts between the plasmasphere and ionosphere. *Geophysical Research Letters*, 42(10), 3707–3714. <https://doi.org/10.1002/2015GL063699>
- Lu, Q., Ke, Y., Wang, X., Liu, K., Gao, X., Chen, L., & Wang, S. (2019). Two-dimensional general curvilinear particle-in-cell (gcPIC) simulation of rising-tone chorus waves in a dipole magnetic field. *Journal of Geophysical Research: Space Physics*, 124, 4157–4167. <https://doi.org/10.1029/2019JA026586>
- Mauk, B. H., Fox, N. J., Kanekal, S. G., Kessel, R. L., Sibeck, D. G., & Ukhorskiy, A. (2013). Science objectives and rationale for the radiation belt storm probes mission. *Space Science Reviews*, 179(1–4), 3–27. <https://doi.org/10.1007/s11214-012-9908-y>
- Meredith, N. P., Horne, R. B., & Anderson, R. R. (2001). Substorm dependence of chorus amplitudes: Implications for the acceleration of electrons to relativistic energies. *Journal of Geophysical Research*, 106(A7), 13165–13178. <https://doi.org/10.1029/2000ja900156>
- Mourenas, D., Artemyev, A., Agapitov, O., & Krasnoselskikh, V. (2012). Acceleration of radiation belts electrons by oblique chorus waves. *Journal of Geophysical Research*, 117(A10), A10212. <https://doi.org/10.1029/2012ja018041>
- Ni, B., Thorne, R. M., Shprits, Y. Y., & Bortnik, J. (2008). Resonant scattering of plasma sheet electrons by whistler-mode chorus: Contribution to diffuse auroral precipitation. *Geophysical Research Letters*, 35(11), L11106. <https://doi.org/10.1029/2008gl034032>
- Nishimura, Y., Bortnik, J., Li, W., Thorne, R. M., Lyons, L. R., Angelopoulos, V., et al. (2010). Identifying the driver of pulsating aurora. *Science*, 330(6000), 81–84. <https://doi.org/10.1126/science.1193186>
- Ohta, K., Kitagawa, T., Shima, N., Hayakawa, M., & Dowden, R. L. (1996). Characteristics of mid-latitude whistler ducts as deduced from ground-based measurements. *Geophysical Research Letters*, 23(23), 3301–3304. <https://doi.org/10.1029/96gl03253>
- Omura, Y., Hikishima, M., Katoh, Y., Summers, D., & Yagitani, S. (2009). Nonlinear mechanisms of lower-band and upper-band VLF chorus emissions in the magnetosphere. *Journal of Geophysical Research*, 114(A7), A07217. <https://doi.org/10.1029/2009ja014206>
- Preece, W. H. (1894). Earth Currents. *Nature*, 49(1276), 554. <https://doi.org/10.1038/049554b0>
- Santolík, O., Gurnett, D. A., Pickett, J. S., Parrot, M., & Cornilleau-Wehrin, N. (2005). Central position of the source region of storm-time chorus. *Planetary and Space Science*, 53(1–3), 299–305. <https://doi.org/10.1016/j.pss.2004.09.056>
- Santolík, O., Macúšová, E., Kolmašová, I., Cornilleau-Wehrin, N., & de Conchy, Y. (2014). Propagation of lower-band whistler-mode waves in the outer Van Allen belt: Systematic analysis of 11 years of multi-component data from the Cluster spacecraft. *Geophysical Research Letters*, 41(8), 2729–2737. <https://doi.org/10.1002/2014gl059815>
- Santolík, O., Parrot, M., & Lefeuvre, F. (2003). Singular value decomposition methods for wave propagation analysis. *Radio Science*, 38(1), 1010. <https://doi.org/10.1029/2000rs002523>
- Santolík, O., Pickett, J. S., Gurnett, D. A., Menietti, J. D., Tsurutani, B. T., & Verkhoglyadova, O. (2010). Survey of Poynting flux of whistler mode chorus in the outer zone. *Journal of Geophysical Research*, 115(A7), A00F13. <https://doi.org/10.1029/2009ja014925>
- Shi, R., Li, W., Ma, Q., Green, A., Kletzing, C. A., Kurth, W. S., et al. (2019). Properties of whistler mode waves in earth's plasmasphere and plumes. *Journal of Geophysical Research Space Physics*, 124(2), 1035–1051. <https://doi.org/10.1029/2018ja026041>
- Shue, J. H., Nariyuki, Y., Katoh, Y., Saito, S., Kasahara, Y., Hsieh, Y. K., et al. (2019). A systematic study in characteristics of lower band rising-tone chorus elements. *Journal of Geophysical Research Space Physics*, 124(11), 9003–9016. <https://doi.org/10.1029/2019ja027368>
- Smith, R. L., Helliwell, R. A., & Yabroff, I. W. (1960). A theory of trapping of whistlers in field-Aligned columns of enhanced ionization. *Journal of Geophysical Research*, 65(3), 815–823. <https://doi.org/10.1029/jz065i003p00815>
- Stenzel, R. L. (1999). Whistler waves in space and laboratory plasmas. *Journal of Geophysical Research*, 104(A7), 14379–14395. <https://doi.org/10.1029/1998ja900120>
- Streltsov, A. V., Lampe, M., & Ganguli, G. (2007). Whistler propagation in nonsymmetrical density channels. *Journal of Geophysical Research*, 112(A6). <https://doi.org/10.1029/2006ja012093>
- Streltsov, A. V., Lampe, M., Manheimer, W., Ganguli, G., & Joyce, G. (2006). Whistler propagation in inhomogeneous plasma. *Journal of Geophysical Research*, 111(A3), A03216. <https://doi.org/10.1029/2005ja011357>
- Summers, D., Omura, Y., Miyashita, Y., & Lee, D. H. (2012). Nonlinear spatiotemporal evolution of whistler mode chorus waves in Earth's inner magnetosphere. *Journal of Geophysical Research*, 117, A09206. <https://doi.org/10.1029/2012ja017842>
- Su, Z., Liu, N., Zheng, H., Wang, Y., & Wang, S. (2018). Large-amplitude extremely low frequency hiss waves in plasmaspheric plumes. *Geophysical Research Letters*, 45(2), 565–577. <https://doi.org/10.1002/2017gl076754>
- Taubenschuss, U., Santolík, O., Breuillard, H., Li, W., & Le Contel, O. (2016). Poynting vector and wave vector directions of equatorial chorus. *Journal of Geophysical Research: Space physics*, 121(12), 11912–11928. <https://doi.org/10.1002/2016ja023389>
- Thorne, R. M., Li, W., Ni, B., Ma, Q., Bortnik, J., Chen, L., et al. (2013). Rapid local acceleration of relativistic radiation-belt electrons by magnetospheric chorus. *Nature*, 504(7480), 411–414. <https://doi.org/10.1038/nature12889>
- Thorne, R. M., Ni, B., Tao, X., Horne, R. B., & Meredith, N. P. (2010). Scattering by chorus waves as the dominant cause of diffuse auroral precipitation. *Nature*, 467(7318), 943–946. <https://doi.org/10.1038/nature09467>

- Tsurutani, B. T., & Smith, E. J. (1974). Postmidnight chorus: A substorm phenomenon. *Journal of Geophysical Research*, 79(1), 118–127. <https://doi.org/10.1029/ja079i001p00118>
- Tsurutani, B. T., & Smith, E. J. (1977). Two types of magnetospheric ELF chorus and their substorm dependences. *Journal of Geophysical Research*, 82(32), 5112–5128. <https://doi.org/10.1029/ja082i032p05112>
- Van Compernelle, B., An, X., Bortnik, J., Thorne, R. M., Pribyl, P., & Gekelman, W. (2015). Excitation of chirping whistler waves in a laboratory plasma. *Physical Review Letters*, 114(24), 245002. <https://doi.org/10.1103/physrevlett.114.245002>
- Wygant, J. R., Bonnell, J. W., Goetz, K., Ergun, R. E., Mozer, F. S., Bale, S. D., et al. (2013). The electric field and waves instruments on the radiation belt storm probes mission. *Space Science Reviews*, 179(1–4), 183–220.
- Zhang, S., Tian, A., Degeling, A. W., Shi, Q., Wang, M., Hao, Y., et al. (2019). Pc4-5 Poloidal ULF Wave Observed in the Dawnside Plasmaspheric Plume. *Journal of Geophysical Research: Space Physics*, 124(12), 9986–9998. <https://doi.org/10.1029/2017ja027319>